Mass-spectrometry of single mammalian cells quantifies proteome heterogeneity during cell differentiation

Bogdan Budnik,[1] Ezra Levy,[2] Nikolai Slavov[2,3]
[1]MSPRL, FAS Division of Science, Harvard University, Cambridge, MA 02138, USA
[2]Department of Biology, Northeastern University, Boston, MA 02115, USA
[3]Department of Bioengineering, Northeastern University, Boston, MA 02115, USA

Cellular heterogeneity is important to biological processes, including cancer and development. However, proteome heterogeneity is largely unexplored because of the limitations of existing methods for quantifying protein levels in single cells. To alleviate these limitations, we developed Single Cell ProtEomics by Mass Spectrometry (SCoPE-MS), and validated its ability to identify distinct human cancer cell types based on their proteomes. We used SCoPE-MS to quantify over a thousand proteins in differentiating mouse embryonic stem (ES) cells. The single-cell proteomes enabled us to deconstruct cell populations and infer protein abundance relationships. Comparison between single-cell proteomes and transcriptomes indicated coordinated mRNA and protein covariation. Yet many genes exhibited functionally concerted and distinct regulatory patterns at the mRNA and the protein levels, suggesting that post-transcriptional regulatory mechanisms contribute to proteome remodeling during lineage specification, especially for developmental genes. SCoPE-MS is broadly applicable to measuring proteome configurations of single cells and linking them to functional phenotypes, such as cell type and differentiation potentials.

Cellular systems, such as tissues, cancers, and cell cultures, consist of a variety of cells with distinct molecular and functional properties. Characterizing such cellular differences is key to understanding normal physiology, combating cancer recurrence (1, 2), and enhancing targeted differentiation for regenerative therapies (3); it demands quantifying the proteomes of single cells.

However, quantifying proteins in single mammalian cells remains confined to fluorescent imaging and antibodies. Fluorescent proteins have proved tremendously useful but are limited to quantifying only a few proteins per cell and sometimes introduce artifacts (4). Multiple methods for quantifying proteins in single cells have been recently developed, including single-cell Western blots (5), CyTOF (6), and Proseek Multiplex, an immunoassay readout by PCR (7). These methods enabled quantifying up to a few dozen endogenous proteins but their throughput and accuracy are limited by the availability of highly-specific antibodies that bind their cognate proteins stoichiometrically. Recent advances have pushed the sensitivity of Mass Spectrometry (MS) to proteins from hundreds of mammalian cells (8), single human oocytes (9) and frog embryos (10) but these small samples still exceed the protein content of a typical mammalian cell ($\sim 15\mu m$ diameter) by orders of magnitude (11).

We aimed to overcome these limitations by developing a high-throughput method for Single Cell ProtEomics by Mass Spectrometry (SCoPE-MS) that can quantify thousands of proteins in single mammalian cells. To develop SCoPE-MS, we resolved two major challenges: (i) delivering the proteome of a mammalian cell to a MS instrument with minimal protein losses and (ii) simultaneously identifying and quantifying peptides from single-cell samples. To overcome the first challenge, we manually picked live single cells under a microscope and lysed them mechanically (by Covaris sonication in glass microtubes) in phosphate-buffered saline, Fig. 1a. This method was chosen to obviate chemicals that may undermine peptide separation and ionization or sample cleanup that may incur significant losses. The proteins from each cell lysate were quickly denatured at $90\ ^oC$ and digested with trypsin at $45\ ^oC$ overnight, Fig. 1a; see Methods for full experimental details.

To overcome the second challenge, we made novel use of tandem mass tags (TMT). This technology was developed for multiplexing (12), which affords cost-effective high-throughput. Even more crucial to our application, TMT allows quantifying the level of each TMT-labeled

peptide in each sample while identifying its sequence from the total peptide amount pooled across all samples (12). SCoPE-MS capitalizes on this capability by augmenting each single-cell set with a sample comprised of $\sim 100 - 200$ carrier cells that provide enough ions for peptide sequence identification, Fig. 1a. Increasing the number of carrier cells increases peptide identification rates but decreases quantitative precision. The carrier cells also help with the first challenge by reducing losses from single cells, since most of the peptides sticking to tips and tube walls originate from the carrier cells. Thus, the carrier cells help overcome the two major challenges.

Quantification of TMT-labeled peptides relies on reporter ions (RI) whose levels reflect both peptide abundances and noise contributions, such as coisolation interference and background noise (12, 13). The low protein abundance poses extreme challenges to the signal-to-noise ratio (SNR) and requires careful evaluation even of aspects that are well established and validated in bulk MS measurements. To evaluate the contribution of background noise to single-cell RI quantification, we estimated the signal-to-noise ratio (SNR), Fig. S1. The estimates indicated that RI intensities are proportional to the amount of labeled single-cell proteomes, and very low for channels left empty. These data suggest that the signal measured in single cells exceeds the background noise by 10-fold or more. As an added SNR control for every TMT set, SCoPE-MS leaves the 130N channel empty, so that 130N RI reflect both isotopic cross-contamination from channel 131 and the background noise.

To evaluate the ability of SCoPE-MS to distinguish different cell types, we prepared three label-swapped and interlaced TMT sets with alternating single Jurkat and U-937 cells, two blood cancer cell lines with average cell diameter of only $11\ \mu m$ (Fig. 1b). The levels of all 767 proteins quantified in single cells were projected onto their principle components (PC). The two-dimensional projections of single-cell proteomes clustered by cell type and in proximity to the projection of bulk samples from the same cell type (Fig. 1c), suggesting that SCoPE-MS can identify cell types based on their proteomes. Next, we identified proteins whose levels vary less within a cell type than between cell types. Among the 107 proteins showing such trends at FDR $< 2\%$, we plotted the distributions for nine in Fig. 1d.

Given the difficulty of measuring extremely low protein levels, we further evaluated SCoPE-MS data by comparing the mean protein levels in the 12 Jurkat cells from Fig. 1b to bulk estimates,

Fig. S2a. The correlation ($\rho = 0.6$) indicates good agreement despite the noise inherent in single cell measurements. The relative quantification by SCoPE-MS was evaluated by correlating protein fold-changes estimated from different cells and TMT channels (Fig. S2b) and technical replicates generated by quantifying the same single-cell-set twice, each time injecting only 50% (Fig. S2c). The results in Fig. S2b,c show that while SCoPE-MS measurements are noisier than bulk MS measurements, they are reproducible, especially for larger fold-changes.

Next, we quantified single-cell proteome heterogeneity and dynamics during ES cell differentiation. To initiate differentiation, we withdrew leukemia inhibitor factor (LIF) from ES cell cultures and transitioned to suspension culture; LIF withdrawal results in complex and highly heterogeneous differentiation of epiblast lineages in embryoid bodies (EB). We used SCoPE-MS to quantify over a thousand proteins at FDR $= 1\ \%$ (Fig. S3a) and their pair-wise correlations (averaging across single cells) in days 3, 5, and 8 after LIF withdrawal (Fig. 2a). Cells from different days were processed together to minimize batch biases (14).

We first explored protein covariation as reflected in the overrepresentation of functionally related proteins within highly coherent clusters of protein-protein correlations, Fig. 2a. The large clusters on all days are enriched for proteins with biosynthetic functions. This covariation is consistent with the possibility of heterogeneous and asynchronous slowing of cell growth as cells differentiate. The smaller clusters correspond to lineage-specific proteins and more specialized functions.

Next, we projected the proteomes of single cells from all days (190 cells) onto their PCs, Fig. 2b. The projections cluster by date; indeed, PC 1 loading correlate to the days post LIF withdrawal, Fig. S3b. The small clusters of lineage-specific genes (Fig. 2a) suggest that we have quantified proteomes of distinct cell states; thus we attempted to identify cell clusters by projecting the EB proteomes onto their PCs and identifying sets of proteins that are concertedly regulated in each cluster, Fig. 2c,d. The projection resulted in clusters of cells, whose identity is suggested by the dominant proteins in the singular vectors. We identified biological functions over-represented (15) within the distribution of PC loadings and colorcoded each cell based on the average levels of proteins annotated to these functions. The PCs do not correlate to missing data, indicating that our experimental design has overcome challenges common to high-throughput single-cell data (14);

see Methods. These results suggest that SCoPE-MS data can meaningfully classify cell identity for cells from complex and highly heterogeneous populations.

Klein *et al.* (16) recently quantified mRNA heterogeneity during ES differentiation, and we used their inDrop data to simultaneously analyze mRNA and protein covariation and to directly test whether genes coexpressed at the mRNA level are also coexpressed at the protein level. To this end, we computed all pairwise correlations between RNAs (Fig. 3a) and proteins (Fig. 3b) for all genes quantified at both levels in cells undergoing differentiation for 7 and 8 days. Clustering hierarchically the correlation matrices results in 3 clusters of genes. To compare these clusters, we computed the pairwise Jaccard coefficients, defined as the number of genes present in both classes divided by the number of genes present in either class, i.e., intersection/union). The results (Fig. 3c) indicate that the largest (green) cluster is 55 % identical and the medium (blue) cluster is 33 % identical. This cluster stability is also reflected in a positive correlation between corresponding mRNA and protein correlations, Fig. 3d. The magnitude of this correlation is comparable to protein-mRNA correlations from bulk datasets (15, 17) and testifies strongly for the quantitative accuracy of both inDrop and SCoPE-MS.

Having established a good overall concordance between mRNA and protein covariation, we next explored whether and how much this concordance varies between genes with different biological functions. The covariation concordance of a gene was estimated as the similarity of its mRNA and protein correlations, i.e., the correlation between the corresponding correlation vectors (18). The median concordance of ribosomal proteins (RP) of both the 60S (RPL) and 40S (RPS) is significantly higher than for all genes, Fig. 3e. This result indicates that RPL and RPS genes have significantly ($p < 10^{-20}$) more similar gene-gene correlations at the mRNA and the protein levels than the other quantified genes. Some RPs correlate less well to the remaining RPs (Fig. S4), which may reflect lineage specific ribosome remodeling, but this possibility needs to be evaluated more directly with isolated ribosomes (19). In contrast to RPs, genes functioning in tissue morphogenesis, proteolysis, and development have significantly ($p < 10^{-3}$) lower concordance at the mRNA and protein level than all genes, Fig. 3e.

The power of MS proteomics had been circumscribed to bulk samples. Indeed, the TMT manufacturer recommends $100\ \mu g$ of protein per channel, almost 10^6 more than the protein content

of a typical mammalian cell (11). SCoPE-MS bridged this gap by efficient sample preparation and the use of carrier cells. These innovations open the gates to further improvements (e.g., increased multiplexing) that will make single-cell MS proteomics increasingly powerful.

SCoPE-MS enabled us to classify cells and explore the relationship between mRNA and protein levels in single mammalian cells. This first foray into single mammalian proteomes demonstrates that mRNA covariaion is predictive of protein covariaion even in single cells. It further establishes the promise of SCoPE-MS to quantitatively characterize single-cell gene regulation and classify cell types based on their proteomes.

Acknowledgments: We thank S. Semrau, M. Jovanovic, R. Zubarev, and members of the Slavov laboratory for discussions and constructive comments, as well as the Harvard University FAS Science Operations for supporting this research project. This work was funded by startup funds from Northeastern University and a New Innovator Award from the NIGMS from the National Institutes of Health to N.S. under Award Number DP2GM123497.

Competing Interests: The authors declare that they have no competing financial interests.

Contributions: B.B., and N.S. conceived the research. B.B., E.L. and N.S. performed experiments and collected data; N.S. analyzed the data and wrote the manuscript.

The raw MS data have been deposited in MassIVE (ID: MSV000080489) and in the ProteomeX change (ID: 0000398). Supplemental website can be found at:
http://www.northeastern.edu/slavovlab/2016_SCoPE-MS/

Figure Captions

Figure 1 | Validating SCoPE-MS by classifying single cancer cells based on their proteomes. (**a**) Conceptual diagram and work flow of SCoPE-MS. Individually picked live cells are lysed by sonication, the proteins in the lysates are digested with trypsin, the resulting peptides labeled with TMT labels, combined and analyzed by LC-MS/MS (Orbitrap Elite). (**b**) Design of control experiments used to test the ability of SCoPE-MS to distinguish U-937 cells from Jurkat cells. Each set was prepared and quantified on a different day to evaluate day-to-day batch artifacts. (**c**) Unsupervised principal component (PC) analysis using data for quantified proteins from the experiments described in panel (b) stratifies the proteomes of single cancer cells by cell type. Protein levels from 6 bulk samples from Jurkat and U-937 cells are also projected and marked with filled semitransparent circles. (**d**) Distributions of protein levels across single U-937 and Jurkat cells indicate cell-type-specific protein abundances.

Figure 2 | Identifying protein covariation and cell clusters across differentiating ES cells. (**a**) Clustergrams of pairwise protein-protein correlations in cells differentiating for 3, 5, and 8 days after LIF withdrawal. The correlation vectors were hierarchically clustered based on the cosine of the angles between them. (**b**) The proteomes of all single EB cells were projected onto their PCs, and the marker of each cell color-coded by day. The single-cell proteomes cluster by day, a trend also reflected in the distributions of PC 1 loadings by day, Fig. S2. (**c, d**) The proteomes of cells differentiating for 8 days were projected onto their PCs, and the marker of each cell color-coded based on the normalized levels of all proteins from the indicated gene-ontology groups.

Figure 3 | Coordinated mRNA and protein covariation in differentiating ES cells. (**a**) Clustergram of pairwise correlations between mRNAs with 2.5 or more reads per cell as quantified by inDrop in single EB cells (16). (**b**) Clustergram of pairwise correlations between proteins quantified by SCoPE-MS in 12 or more single EB cells. (**c**) The overlap between corresponding RNA from (a) and protein clusters from (b) indicates similar clustering patterns. (**d**) Protein-protein correlations correlate to their corresponding mRNA-mRNA correlations. Only genes with significant mRNA-mRNA correlations were used for this analysis. (**e**) The concordance between corresponding mRNA and protein correlations (computed as the correlation between between corresponding correlations (18)) is high for ribosomal proteins (RPL and RPS) and lower for developmental genes; distribution medians are marked with red pluses. Only the subset of genes quantified at both RNA and protein levels were used for all panels.

Methods

Cell culture Mouse embryonic stem cells (E14 10th passage) were grown as adherent cultures in 10 cm plates with 10 ml Knockout DMEM media supplemented with 10 % ES certified FBS, nonessential amino acids (NEAA supplement), 2 mM L-glutamine, 110 $\mu M \beta$-mercapto-ethanol, 1 % penicillin and streptomycin, and leukemia inhibitory factor (mLIF; 1,000 U LIF/ml). ES cells were passaged every two days using StemPro Accutase on gelatin coated tissue culture plates. ES differentiation was triggered by passaging the ES cells into media lacking mLIF in low adherence plates and growing the cells as suspension cultures. Jurkat and U937 cells were grown as suspension cultures in RPMI medium (HyClone 16777-145) supplemented with 10% FBS and 1% pen/strep. Cells were passaged when a density of 10^6 cells/ml was reached, approximately every two days.

Harvesting cells for SCoPE-MS To harvest cells, embryoid bodies were dissociated by treatment with StemPro Accutase (ThermoFisher #A1110501) and gentle pipetting. Cell suspensions of differentiating ES cells, Jurakt cells or U-937 cells were pelleted and washed quickly with cold phosphate buffered saline (PBS). The washed pellets were diluted in PBS at 4 ^oC. The cell density of each sample was estimated by counting at least 150 cells on a hemocytometer, and an aliquot corresponding to 200 cells was placed in a Covaris tube, to be used for the carrier channel. For picking single cells, two $200\mu l$ pools of PBS were placed on a cooled glass slide. Into one of the pools, $2\mu l$ of the cell dilution was placed and mixed, to further dilute the solution. A single cell was then picked under a microscope into a micropipette from this solution. Then, to verify that only one cell was picked, the contents of the micropipette were ejected into the other pool of PBS, inspected, then taken back into the pipette and placed in a chilled Covaris microTUBE-15. Cell-samples in Covaris microtubes were frozen as needed before cell lysis and labeling.

Cell lysis and digestion Each sample – containing a single cell or carrier cells – was lysed by sonication in a Covaris S20 instrument (Woburn, MA) (8). Samples were sonicated for 180s at 125 W power with 10% peak duty cycle, in a degassed water bath at 6 ^oC. During the sonication, samples were shaken to coalesce droplets and bring them down to the bottom of the tube. After lysis, the samples were heated for 15 min at 90 ^oC to denature proteins. Then, the samples were spun at 3000 rpm for 1 min, and ($50ng/\mu l$) trypsin was added; $0.5\mu l$ to single cells and $1\mu l$

to carrier cells. The samples were digested overnight, shaking at 45 ^oC. Once the digest was completed, each samples was labeled with $1\mu l$ of 85mM TMT label (TMT10 kit, Thermo-Fisher, Germany). The samples were shaken for 1 hour in a tray at room temperature. The unreacted TMT label in each sample was quenched with $0.5\mu l$ of 5% hydroxylamine for 15 min according to manufacturers protocol. The samples corresponding to one TMT10 plex were then mixed in a single glass HPLC vial and dried down to 10 μl in a speed-vacuum (Eppendorf, Germany) at 35^oC.

Bulk set The six bulk samples of Jurkat and U-937 cells contained 2,500 cells per sample. The cells were harvested, lysed and processed using the same procedure as for the single cells but with increased amount of trypsin and TMT labels. The samples were labeled, mixed and run as a 6-plex TMT set.

Mass spectrometry analysis Each TMT labeled set of samples was submitted for single LC-MS/MS experiment that was performed on a LTQ Orbitrap Elite (Thermo-Fisher) equipped with Waters (Milford, MA) NanoAcquity HPLC pump. Peptides were first trapped and washed onto a 5cm x 150μm inner diameter microcapillary trapping column packed with C18 Reprosil resin (5 μm, 10 nm, Dr. Maisch GmbH, Germany). The peptides were separated by analytical column 20cm x 75 μm of C18 TPP beads (1.8 μm, 20 nm, Waters, Milford, MA). Separation was achieved through applying an active gradient from $7 - 27$ % ACN in 0.1 % formic acid over 170 min at 200 nl/min. The active gradient was followed by a 10 min $27 - 97$ % ACN wash step. Electrospray ionization was enabled through applying a voltage of 1.8 kV using a home-made electrode junction at the end of the microcapillary column and sprayed from fused silica pico-tips (20 μm ID, 15 μm tip end New Objective, MA). The LTQ Orbitrap Elite was operated in data-dependent mode for the mass spectrometry methods. The mass spectrometry survey scan (MS1) was performed in the Orbitrap in the range of 395 - 1,800 m/z at a resolution of 6×10^4, followed by the selection of up to twenty most intense ions (TOP20) for HCD-MS2 fragmentation in the Orbitrap using the following parameters: precursor isolation width window of 2 m/z, AGC setting of 100,000, a maximum ion accumulation time of 150ms or 250ms, and 6×10^4 resolving power. Singly-charged and and 4+ charge ion species were excluded from HCD fragmentation. Normalized collision energy was set to 37 V and an activation time of 1 ms. Ions in a 7.5 ppm m/z window around ions selected for

MS2 were excluded from further selection for fragmentation for 20 s.

Analysis of raw MS data Raw data were searched by MaxQuant (20) 1.5.7.0 against a protein sequence database including all entries from a SwissProt database and known contaminants such as human keratins and common lab contaminants. The SwissProt databases were the human SwissProt database for the U-937 and the Jurkat cells and the mouse SwissProt database for the differencing ES cells. We also searched all data against subsets of the SwissProt databases comprised from all proteins for which MaxQuant had identified at least one peptide across many single-cell sets in searches against the full SwissProt databases. Theses reduced fasta databases contained 5,267 proteins for mouse and 4,961 proteins for human. MaxQuant searches were performed with trypsin specificity, allowing up to two missed cleavages. TMT tags on peptide N-termini and lysine residues (+229.162932 Da) were set as fixed modifications while methionine oxidation (+15.99492 Da) was set as variable modification. All peptide-spectrum-matches (PSMs) and peptides found by MaxQuant were exported in the msms.txt and the evidence.txt files. Peptides were filtered to 3 % FDR computed as the mean of the posterior error probability (PEP) of all peptides below the cutoff threshold. All razor peptides were used for quantifying the proteins to which they were assigned by MaxQuant.

Data analysis We estimated relative peptide/protein levels from the TMT reporter ions (RI), and protein abundances from the precursor areas distributed according to the RI levels. While such estimates are well validated with bulk samples, extremely low input amounts pose unique challenges that may result in artifacts, e.g., RI intensities may reflect only background noise or the isotopic impurities of TMT tags may cross contaminate TMT channels. We evaluated the degree of background noise and found it significantly below the signal coming from the labeled peptides; see Fig. S1. The relative level of each quantified protein was estimated as the median of the relative levels of its razor peptides. All analysis relied on relative levels, i.e., the level of protein in a cell relative to its mean or median level across all cells in which the protein is quantified. Missing peptide and protein levels were imputed using the k-nearest neighbors algorithm, with k being set to one and the similarity measure for distance being the cosine of the angle between the proteome vectors.

References

1. M. Dean, T. Fojo, S. Bates, *Nature Reviews Cancer* **5**, 275 (2005).

2. A. A. Cohen, *et al.*, *Science* **322**, 1511 (2008).

3. S. Semrau, A. van Oudenaarden, *Annual review of cell and developmental biology* **31**, 317 (2015).

4. D. Landgraf, B. Okumus, P. Chien, T. A. Baker, J. Paulsson, *Nature methods* **9**, 480 (2012).

5. A. J. Hughes, *et al.*, *Nature methods* **11**, 749 (2014).

6. S. C. Bendall, *et al.*, *Science* **332**, 687 (2011).

7. S. Darmanis, *et al.*, *Cell reports* **14**, 380 (2016).

8. S. Li, *et al.*, *Molecular & Cellular Proteomics* **14**, 1672 (2015).

9. I. Virant-Klun, S. Leicht, C. Hughes, J. Krijgsveld, *Molecular & Cellular Proteomics* **15**, 2616 (2016).

10. C. Lombard-Banek, S. A. Moody, P. Nemes, *Angewandte Chemie International Edition* **55**, 2454 (2016).

11. R. Milo, P. Jorgensen, U. Moran, G. Weber, M. Springer, *Nucleic acids research* **38**, D750 (2010).

12. P. L. Ross, *et al.*, *Molecular & cellular proteomics* **3**, 1154 (2004).

13. M. M. Savitski, *et al.*, *Journal of proteome research* **12**, 3586 (2013).

14. S. C. Hicks, M. Teng, R. A. Irizarry, *bioRxiv* **1**, 025528 (2015).

15. A. Franks, E. Airoldi, N. Slavov, *bioRxiv* **1**, DOI: 10.1101/020206 (2016).

16. A. M. Klein, *et al.*, *Cell* **161**, 1187 (2015).

17. M. Wilhelm, *et al.*, *Nature* **509**, 582 (2014).

18. N. Slavov, K. A. Dawson, *Proceedings of the National Academy of Sciences* **106**, 4079 (2009).

19. N. Slavov, S. Semrau, E. Airoldi, B. Budnik, A. van Oudenaarden, *Cell Reports* **13**, 865 (2015).

20. J. Cox, M. Mann, *Nature biotechnology* **26**, 1367 (2008).

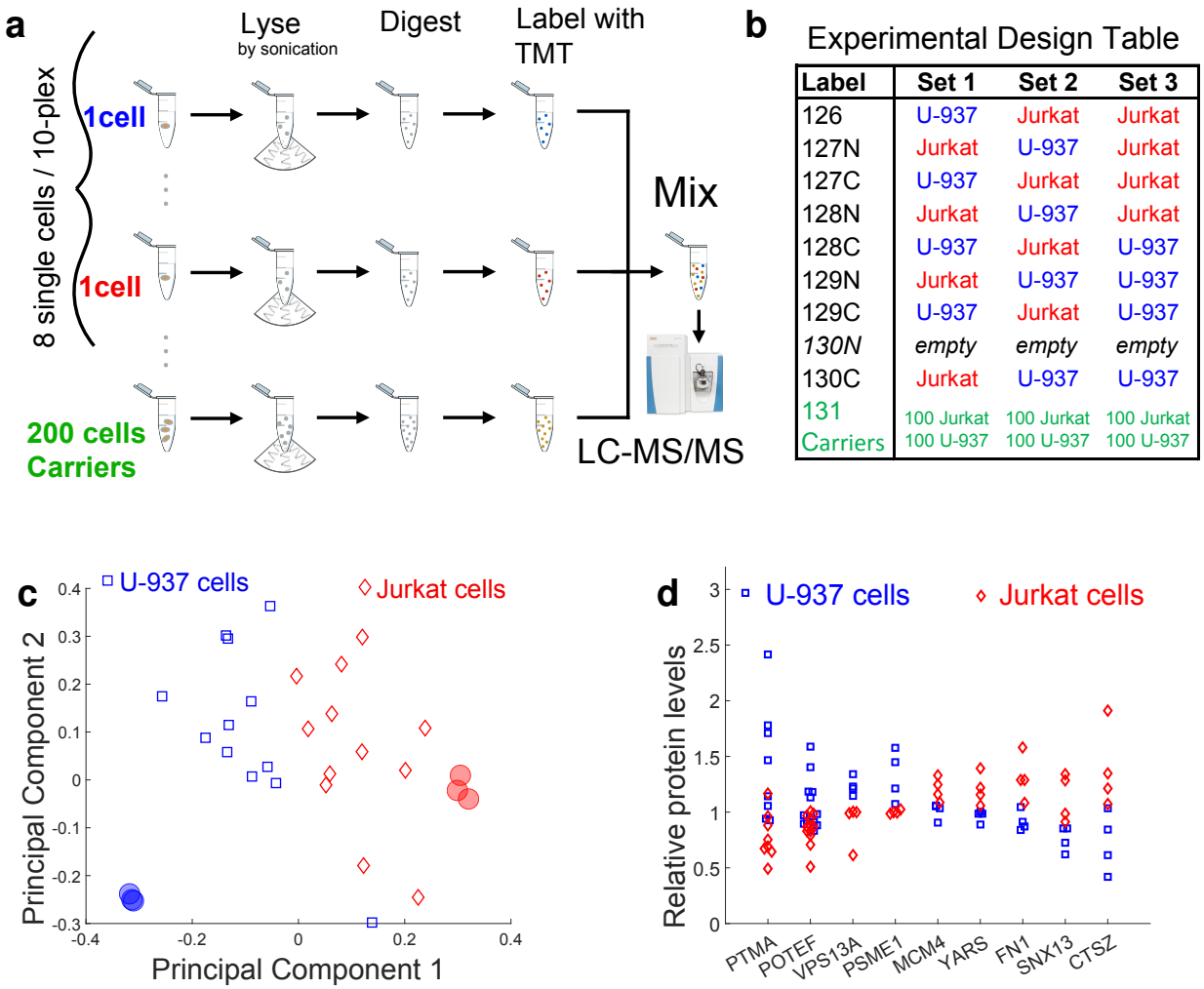

Label	Set 1	Set 2	Set 3
126	U-937	Jurkat	Jurkat
127N	Jurkat	U-937	Jurkat
127C	U-937	Jurkat	Jurkat
128N	Jurkat	U-937	Jurkat
128C	U-937	Jurkat	U-937
129N	Jurkat	U-937	U-937
129C	U-937	Jurkat	U-937
130N	*empty*	*empty*	*empty*
130C	Jurkat	U-937	U-937
131 Carriers	100 Jurkat 100 U-937	100 Jurkat 100 U-937	100 Jurkat 100 U-937

Figure 1 | Validating SCoPE-MS by classifying single cancer cells based on their proteomes. (**a**) Conceptual diagram and work flow of SCoPE-MS. Individually picked live cells are lysed by sonication, the proteins in the lysates are digested with trypsin, the resulting peptides labeled with TMT labels, combined and analyzed by LC-MS/MS (Orbitrap Elite). (**b**) Design of control experiments used to test the ability of SCoPE-MS to distinguish U-937 cells from Jurkat cells. Each set was prepared and quantified on a different day to evaluate day-to-day batch artifacts. (**c**) Unsupervised principal component (PC) analysis using data for quantified proteins from the experiments described in panel (b) stratifies the proteomes of single cancer cells by cell type. Protein levels from 6 bulk samples from Jurkat and U-937 cells are also projected and marked with filled semitransparent circles. (**d**) Distributions of protein levels across single U-937 and Jurkat cells indicate cell-type-specific protein abundances.

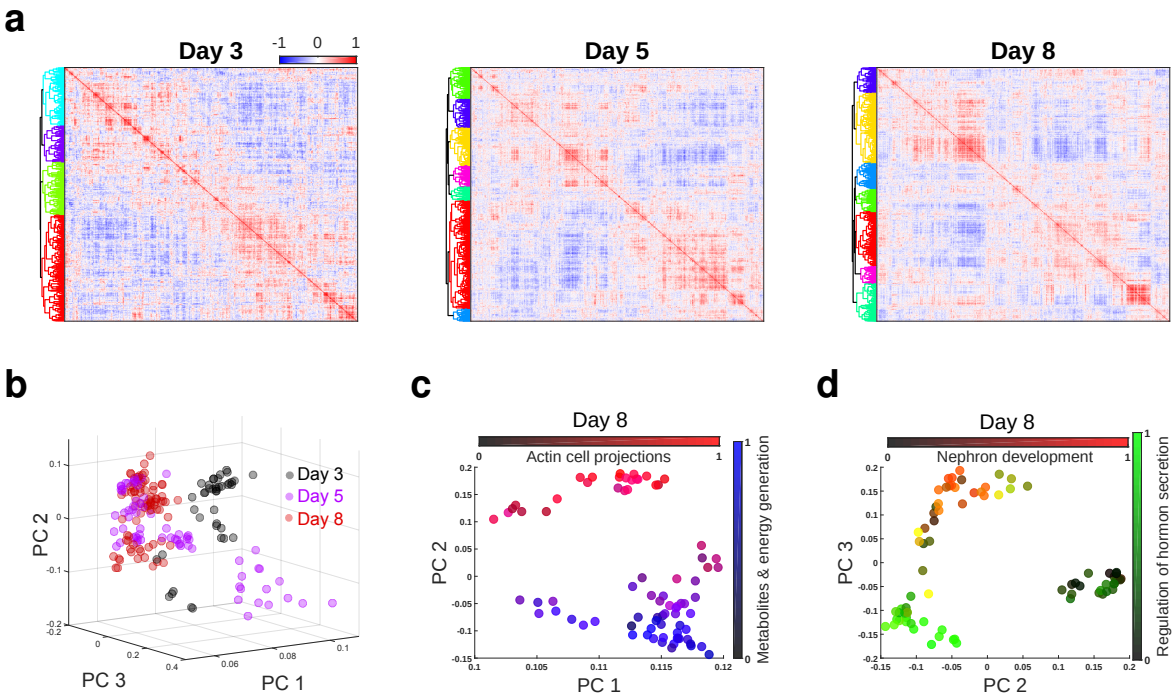

Figure 2 | Identifying protein covariation and cell clusters across differentiating ES cells. (**a**) Clustergrams of pairwise protein-protein correlations in cells differentiating for 3, 5, and 8 days after LIF withdrawal. The correlation vectors were hierarchically clustered based on the cosine of the angles between them. (**b**) The proteomes of all single EB cells were projected onto their PCs, and the marker of each cell color-coded by day. The single-cell proteomes cluster by day, a trend also reflected in the distributions of PC 1 loadings by day, Fig. S2. (**c, d**) The proteomes of cells differentiating for 8 days were projected onto their PCs, and the marker of each cell color-coded based on the normalized levels of all proteins from the indicated gene-ontology groups.

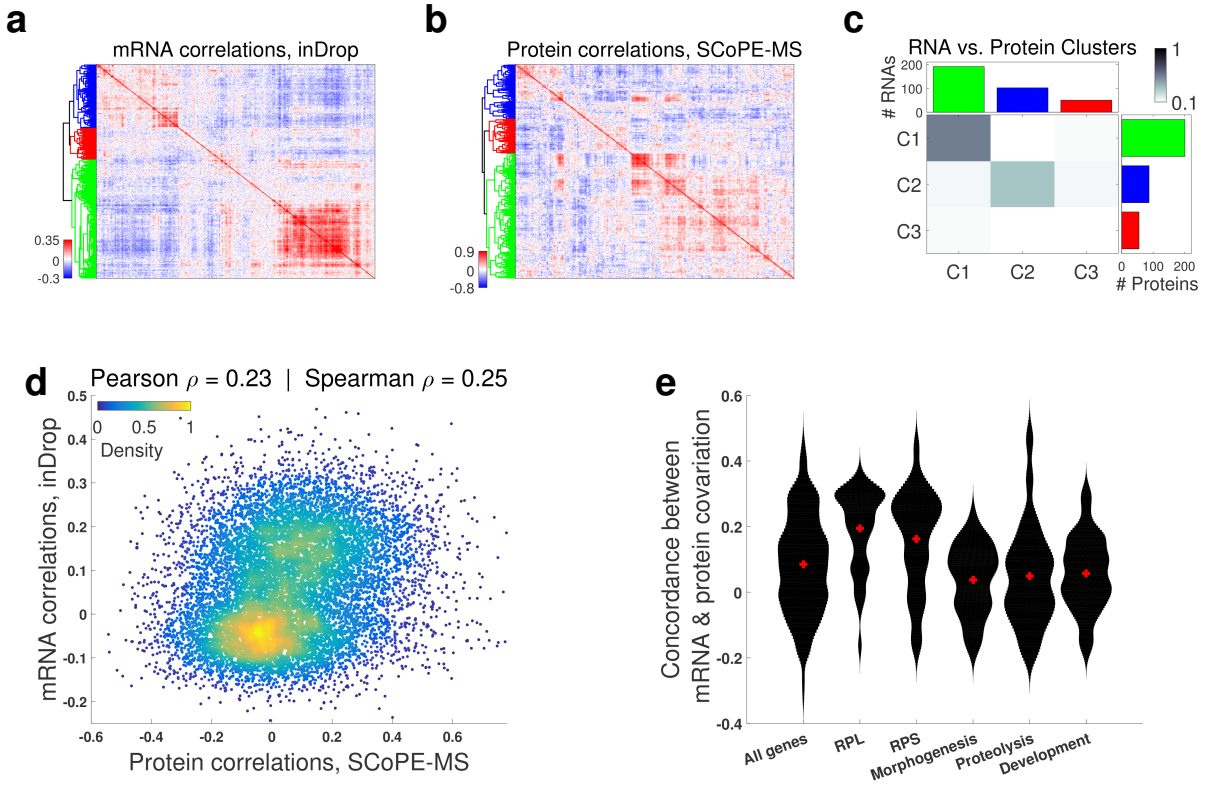

Figure 3 | Coordinated mRNA and protein covariation in differentiating ES cells.
(**a**) Clustergram of pairwise correlations between mRNAs with 2.5 or more reads per cell as quantified by inDrop in single EB cells (16). (**b**) Clustergram of pairwise correlations between proteins quantified by SCoPE-MS in 12 or more single EB cells. (**c**) The overlap between corresponding RNA from (a) and protein clusters from (b) indicates similar clustering patterns. (**d**) Protein-protein correlations correlate to their corresponding mRNA-mRNA correlations. Only genes with significant mRNA-mRNA correlations were used for this analysis. (**e**) The concordance between corresponding mRNA and protein correlations (computed as the correlation between between corresponding correlations (18)) is high for ribosomal proteins (RPL and RPS) and lower for developmental genes; distribution medians are marked with red pluses. Only the subset of genes quantified at both RNA and protein levels were used for all panels.

Supplemental Figures

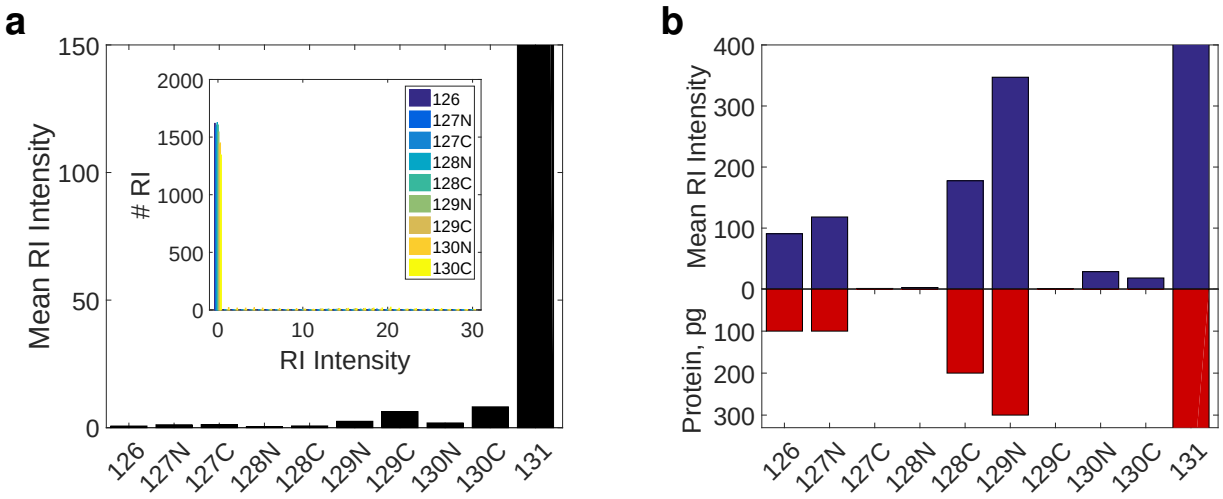

Supplemental Figure 1 | Contribution of background noise to quantification of peptides in single cells. (**a**) Reporter ion (RI) intensities in a SCoPE set in which the single cells were omitted while all other steps were carried out, i.e., trypsin digestion, TMT labeling and addition of carrier cells in channel 131. Thus, RI intensities in channels $126 - 130C$ correspond to background noise. The distribution of RI intensities in the inset shows that the RI for most peptides in channels $126 - 130C$ are zero, i.e., below the MaxQuant noise threshold. The y-axis is limited to 150 to make the mean RI intensities visible. The mean RI intensity for single-cell channels is about 500. (**b**) Mean RI intensities for a TMT set in which only 6 channels contained labeled proteome digests and the other 4 were left empty. Channels 126, 127N, 128C, and 129N correspond to peptides diluted to levels corresponding to 100, 100, 200 and 300 picograms of cellular proteome, channel 131 corresponds to the carrier cells (bars truncated by axes), and the remaining channels were left empty. The RI for most peptides are not detected in the empty channels, and their mean levels very low. This suggests that background noise is low compared to the signal from peptides corresponding to a single cell.

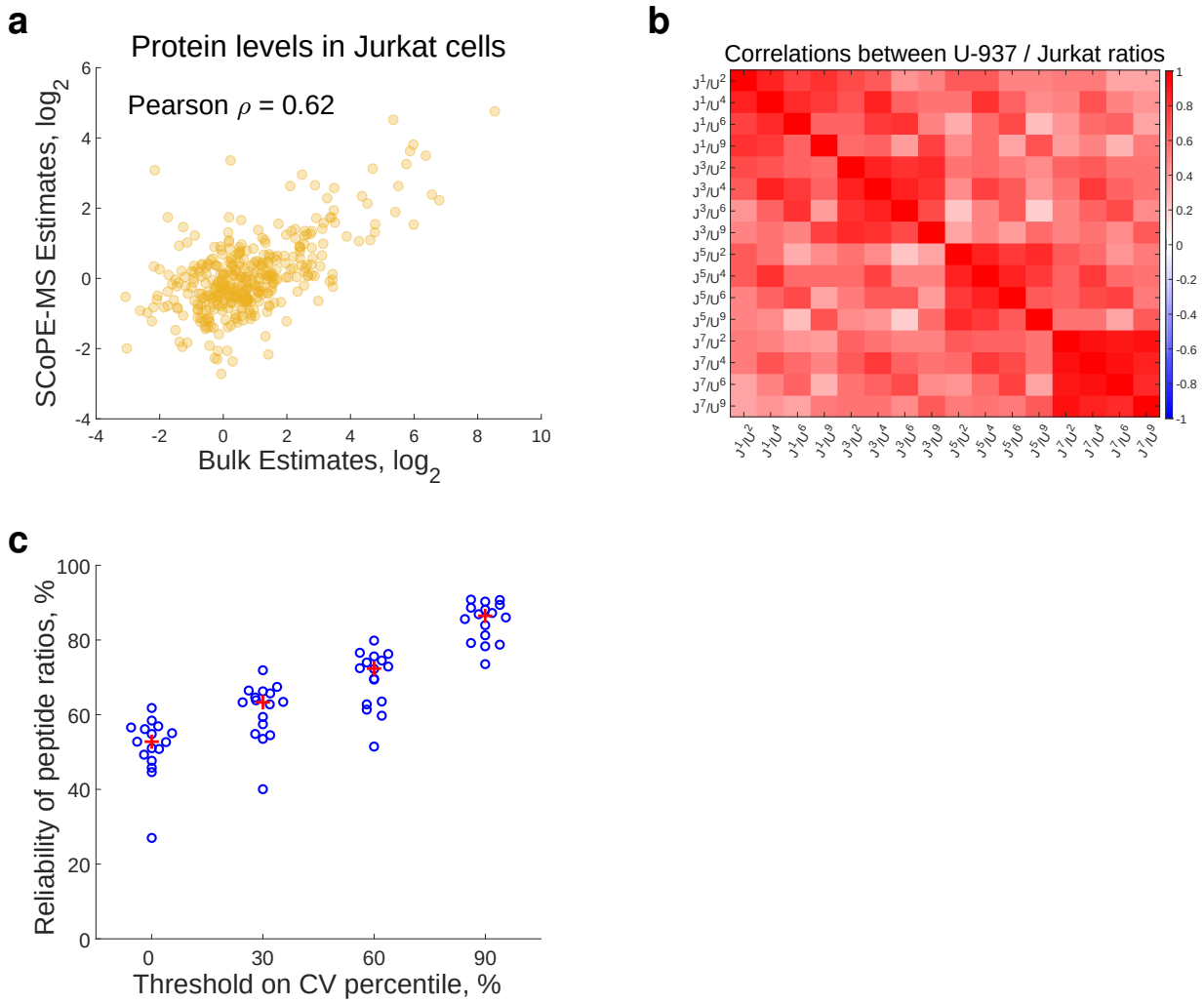

Supplemental Figure 2 | Accuracy of SCoPE-MS quantification. (**a**) Comparison between protein levels estimates from bulk samples of Jurkat cells (x-axis) and from single Jurkat cells (y-axis). The single-cell protein estimates are the average from 12 Jurkat cells from the experiments described in Fig. 1b. Protein levels were estimated as the summed up precursor ion areas apportioned to the reporter ion intensities. (**b**) A correlation matrix of all pairwise Pearson correlations among the ratios of peptide abundances in U-937 and in Jurkat cells from Set 2 in Fig. 1b. The superscripts corresponds to the TMT labels ordered by mass, with 1 being 126, 2 being 127N and so on. The positive correlations among estimates from different combinations of TMT channels suggest good consistency of relative quantification. (**c**) Distributions of correlations between technical replicates of peptide ratios measured in two halves of the same single-cell set; each measurement estimated the peptide ratios from peptides corresponding to 1/2 cell. The first distribution correspond to correlations from across all measured peptides. The other distributions correspond to the correlations computed from the subset of peptides having coefficient of variation (CV) above the indicated percentile, i.e., peptides with larger fold changes. The red crosses mark the distribution medians. All correlations are computed with log transformed protein levels and ratios.

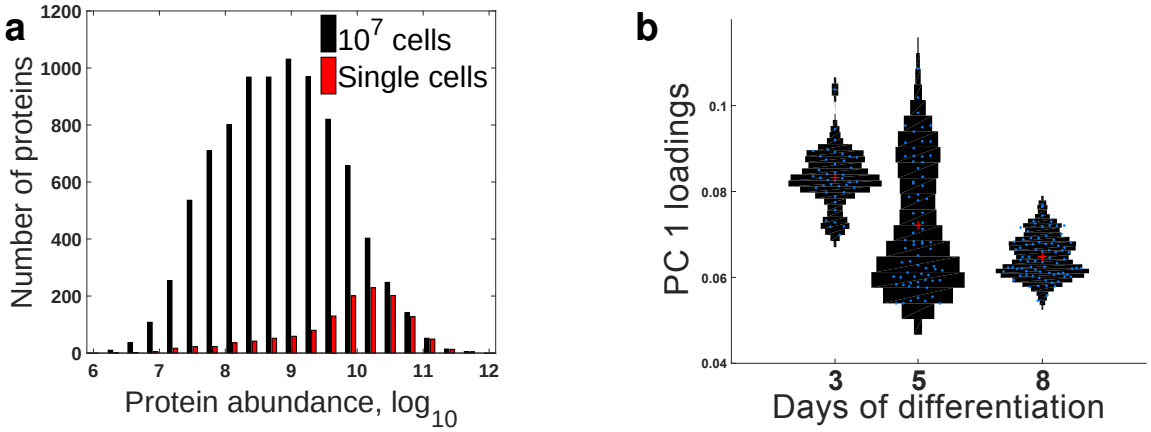

Supplemental Figure 3 | Proteome coverage of differentiating ES cells and distributions of the PC 1 loadings by day of differentiation. (**a**) Distribution of protein abundances for all proteins quantified from 10^7 differentiating ES cells or in at least one single-cell SCoPE-MS set at FDR ≤ 1 %. The probability of quantifying a protein by SCoPE-MS is close to 100 % for the most abundant proteins quantified in bulk samples and decreases with protein abundance, for total of 1526 quantified proteins. (**b**) The proteomes of all differentiating single cells were decomposed into singular vectors and values, and distributions of the loading (elements) of the singular vector with the largest singular value, i.e., PC 1, shown as violin plots. Individual blue circles correspond to single cells, and the red crosses correspond to the medians for each day.

a

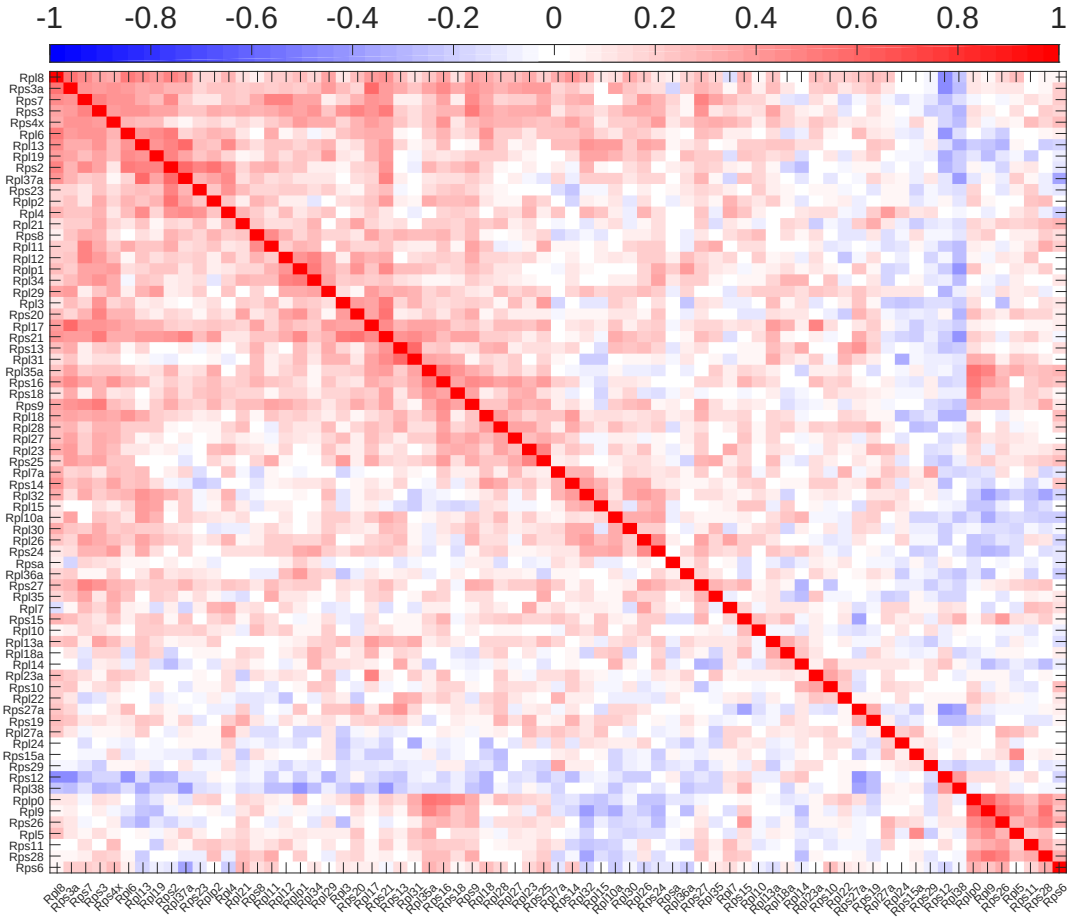

Supplemental Figure 4 | Correlations between ribosomal proteins (**a**) All pairwise Pearson correlations between ribosomal proteins on day 8 were computed by averaging across cells. The correlations matrix was clustered, using the cosine between the correlation vectors as a similarly measure.